arXiv:2405.12370v2 [astro-ph.HE] 25 Jul 2024

Swift J1727.8-1613 has the Largest Resolved Continuous Jet Ever Seen in an X-ray Binary

Callan M. Wood [ID],[1] James C. A. Miller-Jones [ID],[1] Arash Bahramian [ID],[1] Steven J. Tingay [ID],[1]
Steve Prabu [ID],[1] Thomas D. Russell [ID],[2] Pikky Atri [ID],[3] Francesco Carotenuto [ID],[4] Diego Altamirano [ID],[5]
Sara E. Motta [ID],[6] Lucas Hyland [ID],[7] Cormac Reynolds [ID],[8] Stuart Weston,[9] Rob Fender,[4] Elmar Körding,[10]
Dipankar Maitra [ID],[11] Sera Markoff [ID],[12, 13] Simone Migliari,[14] David M. Russell [ID],[15] Craig L. Sarazin [ID],[16]
Gregory R. Sivakoff [ID],[17] Roberto Soria [ID],[18, 19, 20] Alexandra J. Tetarenko [ID],[21] and Valeriu Tudose[22]

[1]*International Centre for Radio Astronomy Research, Curtin University, GPO Box U1987, Perth, WA 6845, Australia*
[2]*INAF, Istituto di Astrofisica Spaziale e Fisica Cosmica, Via U. La Malfa 153, I-90146 Palermo, Italy*
[3]*ASTRON, Netherlands Institute for Radio Astronomy, Oude Hoogeveensedijk 4, 7991 PD Dwingeloo, The Netherlands*
[4]*Astrophysics, Department of Physics, University of Oxford, Keble Road, Oxford, OX1 3RH, UK*
[5]*School of Physics and Astronomy, University of Southampton, University Road, Southampton SO17 1BJ, UK*
[6]*INAF - Osservatorio Astronomico di Brera, Via E. Bianchi 46, I-23807 Merate, Italy*
[7]*Mathematics & Physics, School of Natural Sciences, University of Tasmania, Private Bag 37, Hobart, Tasmania, 7001*
[8]*CSIRO Astronomy and Space Science, P.O. Box 1130, Bentley, WA 6102, Australia*
[9]*Space Operations New Zealand Ltd, Hargest House, PO Box 1306, Invercargill 9840, New Zealand*
[10]*Department of Astrophysics/IMAPP, Radboud University, P.O. Box 9010, 6500 GL Nijmegen, The Netherlands*
[11]*Department of Physics and Astronomy, Wheaton College, Norton, MA 02766, USA*
[12]*Anton Pannekoek Institute for Astronomy, University of Amsterdam, Science Park 904, 1098 XH Amsterdam, The Netherlands*
[13]*Gravitation and Astroparticle Physics Amsterdam Institute, University of Amsterdam, Science Park 904, 1098 XH 195 196 Amsterdam, The Netherlands*
[14]*Aurora Technology, Calle Principe de Vergara, 211, 1-B, E-28002 Madrid, Spain*
[15]*Center for Astrophysics and Space Science (CASS), New York University Abu Dhabi, P.O. Box 129188, Abu Dhabi, UAE*
[16]*Department of Astronomy, University of Virginia, 530 McCormick Road, Charlottesville, VA 22904-4325, USA*
[17]*Department of Physics, University of Alberta, CCIS 4-181, Edmonton AB T6G 2E1, Canada*
[18]*INAF - Osservatorio Astrofisico di Torino, Strada Osservatorio 20, 10025 Pino Torinese, Italy*
[19]*College of Astronomy and Space Sciences, University of the Chinese Academy of Sciences, Beijing 100049, People's Republic of China*
[20]*Sydney Institute for Astronomy, School of Physics A28, The University of Sydney, Sydney, NSW 2006, Australia*
[21]*Department of Physics and Astronomy, University of Lethbridge, Lethbridge, Alberta, T1K 3M4, Canada*
[22]*Institute for Space Sciences, National Institute for Laser, Plasma and Radiation Physics, Atomistilor 409, PO Box MG-23, 077125 Bucharest-Magurele, Romania*

ABSTRACT

Multi-wavelength polarimetry and radio observations of *Swift* J1727.8-1613 at the beginning of its recent 2023 outburst suggested the presence of a bright compact jet aligned in the north-south direction, which could not be confirmed without high angular resolution images. Using the Very Long Baseline Array and the Long Baseline Array, we imaged *Swift* J1727.8-1613 during the hard/hard-intermediate state, revealing a bright core and a large, two-sided, asymmetrical, resolved jet. The jet extends in the north-south direction, at a position angle of $-0.60 \pm 0.07°$ East of North. At 8.4 GHz, the entire resolved jet structure is $\sim 110(d/2.7\,\mathrm{kpc})/\sin i$ AU long, with the southern approaching jet extending $\sim 80(d/2.7\,\mathrm{kpc})/\sin i$ AU from the core, where d is the distance to the source and i is the inclination of the jet axis to the line of sight. These images reveal the most resolved continuous X-ray binary jet, and possibly the most physically extended continuous X-ray binary jet ever observed. Based on the brightness ratio of the approaching and receding jets, we put a lower limit on the intrinsic jet speed of $\beta \geq 0.27$ and an upper limit on the jet inclination of $i \leq 74°$. In our first observation we also detected a rapidly fading discrete jet knot 66.89 ± 0.04 mas south of the core, with a proper motion of 0.66 ± 0.05

Corresponding author: Callan M. Wood
callan.wood@icrar.org

mas hour^{-1}, which we interpret as the result of a downstream internal shock or a jet-ISM interaction, as opposed to a transient relativistic jet launched at the beginning of the outburst.

1. INTRODUCTION

Black hole low-mass X-ray binaries (BH LMXBs) are ideal systems to study the launching of relativistic jets and their connection to the processes of accretion, due to their proximity and variability on human timescales. The properties of relativistic jets are strongly coupled to the properties of the accretion inflow, which both evolve dramatically and rapidly during bright outbursts.

Typical BH LMXB outbursts begin in a rising hard state, where the radio emission is dominated by a compact, steady, partially self-absorbed, synchrotron-emitting, continuous jet (e.g. Corbel et al. 2000; Fender 2001). These hard-state jets[1] become quenched as the source moves towards the transition into the soft state, via intermediate states, where bright, discrete transient jet ejecta are often launched (see e.g. Fender et al. 2004, for a review of jets and X-ray binary outbursts). The hard-state jets are often called compact jets, due to their appearance as bright, compact point sources in high angular resolution observations. Resolved hard-state jets have only been observed in a few black hole X-ray binaries: the high-mass X-ray binary Cyg X-1 (Stirling et al. 2001); and the low-mass X-ray binaries GRS 1915+105 (Dhawan et al. 2000; Ribó et al. 2004); MAXI J1836-194 (Russell et al. 2015); and MAXI J1820+070 (Tetarenko et al. 2021).

High angular resolution observations of resolved hard-state jets can provide independent probes of their fundamental jet properties, complementing other methods such as radio and infrared timing studies (e.g. Kalamkar et al. 2016; Malzac et al. 2018; Tetarenko et al. 2019, 2021), astrometry and core shift measurements (e.g. Miller-Jones et al. 2021; Prabu et al. 2023), and broad-band spectral modelling and spectral break studies (e.g. Markoff et al. 2001; Corbel et al. 2002; Chaty et al. 2011; Gandhi et al. 2011; Russell et al. 2014a; Péault et al. 2019; Russell et al. 2020; Echiburú-Trujillo et al. 2024).

1.1. *Swift J1727.8-1613*

Swift J1727.8-1613 (hereafter J1727) was first detected on 2023 August 24 by *Swift*/BAT (Page et al. 2023), with follow-up X-ray observations revealing it to be a new candidate black hole low-mass X-ray binary in the hard-state at the beginning of a bright outburst (Kennea

& Swift Team 2023; Negoro et al. 2023a,b; Nakajima et al. 2023; O'Connor et al. 2023a,b; Castro-Tirado et al. 2023). Optical observations suggested that J1727 has a black hole primary with an early K-type companion star, with an orbital period of $\sim$ 7.6 hours at a distance of $d = 2.7 \pm 0.3$ kpc.

Optical and near-infrared observations of J1727 during the rising hard-state at the beginning of the outburst showed that the source was reddening, possibly due to the onset of a compact hard-state jet (Baglio et al. 2023). Radio observations from the Submillimetre Array (SMA), the Karl G. Jansky Very Large Array (VLA), the enhanced Multi Element Remotely Linked Interferometer (eMERLIN), and the Allen Telescope Array (ATA), showed a bright, flat-spectrum, unresolved source (Vrtilek et al. 2023; Miller-Jones et al. 2023; Baglio et al. 2023; Williams-Baldwin et al. 2023). Polarisation observations at X-ray wavelengths with the Imaging X-ray Polarimetry Explorer (IXPE), at optical wavelengths with the 60 cm Tohoku telescope, at 230 GHz with the SMA, and at 5.5 and 9 GHz with the Australian Telescope Compact Array (ATCA) revealed J1727 to be polarised across the electromagnetic spectrum, with a position angle consistent with being aligned in the north-south direction (Dovciak et al. 2023; Kravtsov et al. 2023; Veledina et al. 2023; Vrtilek et al. 2023; Ingram et al. 2023). These observations suggested that J1727 had a bright, compact, hard-state jet aligned in the north-south direction.

In this letter we present four VLBI observations with the Very Long Baseline Array (VLBA) and the Long Baseline Array (LBA), which reveal the highly extended, resolved, north-south jet of J1727 during the hard/hard-intermediate state, as well as an apparently disconnected discrete jet knot downstream. In Section 2 we detail our observations, calibration, and imaging procedures, and in Section 3 we present our images and perform analysis on the jet, which we discuss in Section 4.

2. OBSERVATION, CALIBRATION, AND IMAGING

Following the beginning of the outburst and the detection of a bright radio counterpart (Miller-Jones et al. 2023), we observed J1727 with the VLBA (project code BM538) at 8.37 GHz on 2023 August 30, as part of the Jet Acceleration and Collimation Probe Of Transient X-Ray Binaries (JACPOT XRB; Miller-Jones et al. 2011b) program. Following that observation, we observed $\sim$ 4 hours later with the LBA (project code V456) at 8.44 GHz, and then twice more on 2023 September 04 and

---

[1] Throughout this letter, we refer to these continuous jets as 'hard-state jets' due to their historical association with the hard state, although they can persist into the hard-intermediate state, but never into the soft state.
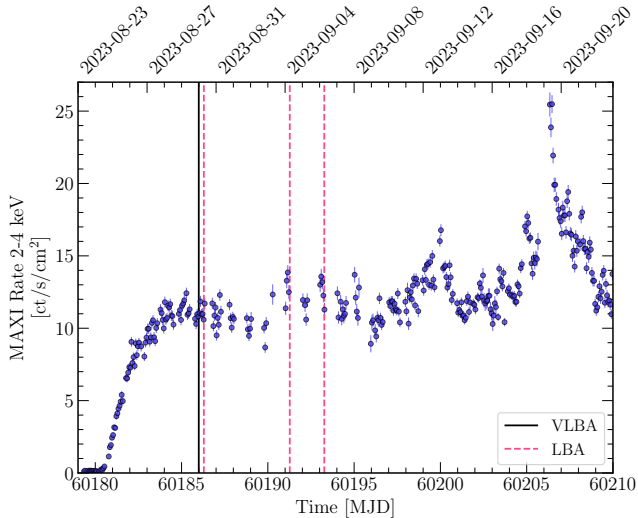
Figure 1. MAXI light curve of the evolution of *Swift* J1727.8-1613 at the beginning of its 2023 outburst. The time of our four VLBI observations are marked by the vertical lines, and their details are given in Table 1.

September 06. Figure 1 shows the timing of our observations during the beginning of the outburst as seen by the Monitor of All-sky X-ray Image (MAXI[2]; Matsuoka et al. 2009) mission. The observation details can be found in Table 1. Further VLBI observations of the evolution of J1727 throughout its outburst will be presented in a future paper (Wood et al. in prep.).

For the VLBA, we used ICRF J174358.8-035004 (J1743-0350) as a fringe finder, ICRF J172134.6-162855 (J1721-1628) as a phase reference source, and ICRF J172446.9-144359 (J1724-2914) as a check source (Charlot et al. 2020). We observed geodetic blocks (Reid et al. 2009) for ∼30 minutes at the beginning and end of the observation to improve astrometric calibration. For the LBA, we used ICRF J192451.0-291430 (B1921-293; Charlot et al. 2020) as a fringe finder. In order to maximise signal-to-noise on the long baselines for phase calibration, we swapped the phase reference and check sources for the LBA. The data were correlated using the DiFX software correlator (Deller et al. 2007, 2011), and calibrated according to the standard procedures within the Astronomical Image Processing System (AIPS, version 31DEC22; Wells 1985; Greisen 2003). After the standard external gain calibration, we performed several rounds of hybrid mapping of the phase reference source to derive the time-varying phase, delay, and rate solutions, which we interpolated to J1727. We also performed a single round of amplitude self-calibration to

get most accurate time-varying amplitude gain calibration, which we applied to J1727. To match the flux density scales of the VLBA and the LBA, we used the VLBA map of J1724-2914 to derive a global amplitude gain solution for each LBA antenna IF, and polarisation to scale the a priori amplitude gains approximated from the zenith system equivalent flux densities. We used the VLBA and LBA scans of J1721-1628 to confirm that the LBA flux density scale matched the VLBA to within 5%.

We imaged J1727 within AIPS using the CLEAN algoritm (Högbom 1974) with natural weighting to maximise sensitivity, and we performed multiple rounds of phase-only self-calibration followed by a single round of amplitude self-calibration to obtain the final images.

3. IMAGES AND ANALYSIS

Figure 2 shows the VLBA image of J1727 from 2023 August 30, which reveals a bright core with a highly resolved, asymmetric jet extending in the north-south direction, and a discrete jet knot to the south at a separation of 66.7 ± 0.2 mas from the core (which we later refined with visibility modelling). The extended continuous structure is a total of ~ 40 mas in length, with the southern and northern jets extending ~ 30 and ~ 10 mas from the core, respectively.

We measured the position of the core in the VLBA image by fitting a point source to the brightest region of the jet using the AIPS task JMFIT, prior to applying any phase self-calibration. This gave a position (in the FK5 reference frame and the J2000 equinox) of

$$\text{R.A.} = 17^{\text{h}}27^{\text{m}}43^{\text{s}}.3135784 \pm 0.0000065,$$

$$\text{Dec.} = -16°12'19''.18042 \pm 0.00033,$$

where the errors are the 1σ statistical errors reported by AIPS added in quadrature with the estimated VLBA systematic astrometric errors (Pradel et al. 2006), and assuming the position of J1721-1628 to be R.A. $= 17^{\text{h}}22^{\text{m}}56^{\text{s}}.498932 \pm 0.000077$, Dec. $= -16°30'19''.26363 \pm 0.00072$.

By fitting a constant position angle to the locations of the positive flux density CLEAN components in the VLBA observations, we measured the position angle of the jet to be $-0.60\pm0.07°$ East of North. This is consistent with the position angle from the core to the southern discrete jet knot. The jet is unresolved perpendicular to the jet axis for its entire length, so based on the size of the beam and the length of the jet, we place an upper limit on the apparent jet half-opening angle of $< 0.5°$.

In Figure 3 we show all four observations of the resolved jet of J1727. These observations similarly show

Table 1. VLBI observation log of the *Swift* J1727.8-1613 hard-state jet.

Label	Date (2023)	Time (UTC)	MJD (Midpoint)	Telescope	Observation Code	Frequency (GHz)	Bandwidth (MHz)	Stations[†]
VLBA	30 Aug	00:32:46–03:20:37	60186.08	VLBA	BM538A	8.37	512	FD,HN,KP,LA, MK,NL,OV,SC
LBA1	30 Aug	07:05:56–12:46:35	60186.41	LBA	V456H	8.44	64	CD,HB,KE,MP, PA,WW
LBA2	04 Sep	06:35:56–12:19:59	60191.39	LBA	V456I	8.44	64	AT,CD,HB,KE, MP,PA,WW
LBA3	06 Sep	06:36:02–12:19:59	60193.39	LBA	V456J	8.44	64	AT,CD,MP,PA, WW

[†] LBA Stations: CD=Ceduna, HB=Hobart 12m, KE=Katherine, MP=Mopra, PA=Parkes, WW=Warkworth 30m, AT=ATCA

a bright core with an extended jet at the same position angle, however the LBA images have poorer angular resolution than the VLBA image, and thus we only resolve the southern jet. We do not see the southern discrete jet knot in any of the LBA observations. We summarise the observed peak and integrated flux densities of the observations in Table 2. The integrated flux density of the jet decreased from the first observation to the final two observations.

The LBA was slightly more sensitive to diffuse emission than the VLBA, which explains why we recovered slightly more emission at the tip of the southern jet in the first LBA observation than with the VLBA. By imaging the VLBA observation with only the shortest baselines, we were unable to detect any more diffuse emission between the extended jet and the discrete jet knot. We note that the VLBA was missing the Pie Town station, and therefore lacked a few key short baselines, which could explain why we only partially detect the diffuse emission at the tip of the southern continuous jet, causing its knotty appearance. The measured flux densities from our first two observations are consistent with the observations from eMERLIN and the ATA on 2023 August 29 and August 30, respectively (Williams-Baldwin et al. 2023; Bright et al. 2023), to within the ∼10% amplitude calibration uncertainties, suggesting that we have recovered most of the emission of the jet of J1727 in our observations.

For symmetric, continuous, steady-state jets inclined to the line of sight, the approaching and receding jets should be approximately symmetric, however the apparent surface brightness of these jets will be asymmetric due to relativistic aberration. The flux density ratio of approaching and receding continuous jets is given by

$$\frac{S_a}{S_r} = \left(\frac{1 + \beta \cos i}{1 - \beta \cos i} \right)^{2-\alpha}, \qquad (1)$$

where S_a and S_r are the flux densities of the jets at an equal angular separation from the core, and α is the spectral index of the jets ($S_\nu \propto \nu^\alpha$; Ryle & Longair 1967; Scheuer & Readhead 1979; Mirabel & Rodríguez 1999). The emission from the receding jet will fall below the noise limit of an observation at a smaller separation than the approaching component, which explains the asymmetry seen in our images if the northern jet is receding and the southern jet is approaching.

Since the receding jet was only resolved in the VLBA observation, we used this observation to constrain the flux density ratio. The CLEAN components for the northern jet terminated at a separation of 6.5 mas from the core, and so we integrated the flux density of the CLEAN components along the northern and southern jets from 3-6.5 mas separation from the core. We chose the lower limit of 3 mas to avoid the emission of the unresolved core (see Appendix A). This yielded a flux density ratio of 4.8±0.4, which gave $\beta \cos i = 0.29 \pm 0.03$, assuming a spectral index of $\alpha = -0.6 \pm 0.2$ (since the extended jet should be optically thin beyond the core).

3.1. *Modelling the Southern Knot*

By separately imaging the first and second halves of the VLBA observation, we found that the southern knot appeared to be moving away from the core. We were able to precisely measure this motion by implementing the time-dependent model-fitting procedure described in Wood et al. (2023), where we fit a time-evolving model directly to the measured visibilities using the Bayesian inference algorithm nested sampling (Skilling 2006) implemented in the dynesty[3] Python package (Speagle 2020). Before modelling the knot, we subtracted the CLEAN components of the extended jet from the visibilities to create a residual observation containing only

---

[3] https://github.com/joshspeagle/dynesty

Table 2. Summary of the jet image parameters from Figure 3. The core flux density is calculated by fitting a point source to the core. Here we add a 10% amplitude calibration error in quadrature with the 1σ statistical errors reported by AIPS. The statistical error in the integrated flux density is given by $\sigma\sqrt{N_{\mathrm{beam}}}$, where σ is the rms noise in the image and N_{beam} are the number of independent beams in the integrated area.

Observation	Integrated Flux Density (mJy)	Core Flux Density (mJy)	Beam Dimensions (mas) x (mas)	Beam Position Angle (° East of North)
VLBA	101 ± 10	46 ± 5	3.9 x 0.9	-15.7
LBA1	90 ± 16	64 ± 6	7.3 x 3.3	17.7
LBA2	71 ± 8	58 ± 6	7.6 x 4.7	14.0
LBA3	75 ± 8	65 ± 7	9.9 x 1.7	6.5

the southern knot. We then fit an analytical model directly to these residual visibilities, consisting of a circular Gaussian with fixed size moving away from the core at a fixed position angle (θ) with a constant speed ($\dot{r}$). We allowed the flux density (F) of this component to vary linearly within the observation. The flux density evolved as

$$F(t) = F_0 + \dot{F}(t - t_0), \qquad (2)$$

and the position of the knot relative to the core as

$$\Delta x(t) = (r_0 + \dot{r}(t - t_0))\sin\theta, \qquad (3)$$

and

$$\Delta y(t) = (r_0 + \dot{r}(t - t_0))\cos\theta, \qquad (4)$$

where t_0 is the reference time chosen as the approximate midpoint of the observation (02:00:00 UTC on 2023 August 30th), r_0 is the separation of the jet knot from the core (in mas) at the reference time, and Δx and Δy are in the directions of positive R.A. and Dec., respectively (in mas). We placed Gaussian priors on the separation of the jet knot at the reference time, and its position angle, based on the location of the knot in the image. We placed uniform priors on all other parameters. The prior distributions are listed in Table 3 along with the posterior estimates. We also tried models that included linear expansion of the jet knot, but found that the expansion speed was consistent with zero. Similarly, we were unable to measure any intra-observational deceleration. We also found that models with exponential or power-law flux density decays were indistinguishable from a linear decay model on the timescale of the ~ 3 hour observation.

We found that the knot was clearly resolved, and was moving away from the core at a proper motion of $\dot{r} = 0.66 \pm 0.05$ mas hour^{-1}, at a position angle consistent with the extended jet position angle. We found that the jet knot was rapidly decaying over the observation, which explains why we do not see the knot in the first LBA observation ~ 4 hours later. Using the separation of the knot and its ballistic speed, we calculated an ejection date of MJD 60181.8 ± 0.2, although

in Section 4.4 we argue that this knot is not a discrete transient jet. The separation and FWHM size of the jet knot in the VLBA observation (see Table 3) give a projected half-opening angle of $0.822 \pm 0.021°$.

To ensure that the process of self-calibration was not corrupting or inducing any false variability in the data, we performed the subtraction and modelling process on versions of the observation without any self-calibration, after phase-only self-calibration, and after amplitude and phase self-calibration. We found that the position and motion of the knot was consistent between all three self-calibration scenarios, and that the size and flux density changed slightly after amplitude self-calibration. We also found marginal evidence of expansion in the observation containing amplitude self-calibration, however we only report the model parameters from the fit to the observation containing phase-only self-calibration, since we could not confirm that the amplitude self-calibration was not inducing false structure and variability in the jet knot.

4. DISCUSSION

We have observed the highly resolved jet of *Swift* J1727.8-1613 over four epochs with the VLBA and the LBA. The jet is continuous, extended, apparently asymmetrical, and aligned in the north-south direction. In the first observation there was also a discrete jet knot moving away from the core to the south, which does not appear in the subsequent observations. We were able to constrain the motion and flux density variability of the jet knot with time-dependent visibility model-fitting.

4.1. *Core Location*

We measured the location of the bright core in the VLBA image, which is likely consistent with the location of the central black hole. In Cyg X-1, where the base of the jet is highly free-free absorbed by the strong stellar wind of the supergiant companion (see e.g. Miller-Jones et al. 2021), the distance between the black hole and the synchrotron photosphere (where the compact "core" emission originates from) is between $\sim 1 - 3 \times 10^{13}$ cm at 8.4 GHz (Zdziarski et al. 2023). Accounting for the

Table 3. Prior distributions and posterior estimates for the moving jet knot in the VLBA observation in Figure 2, using equations 2-4. The reference time is defined as 02:00:00 (UTC) on 2023 August 30th, which is approximately the midpoint of the observation. We report the median of the marginal posterior distributions as the best-fit parameters, and the 16th and 84th percentiles as the uncertainties.

Parameter	Prior Distribution	Posterior Estimate
F_0 (mJy)	$\mathcal{U}(\min = 0, \max = 10)$	4.60 ± 0.10
$\dot{F}$ (mJy hour^{-1})	$\mathcal{U}(\min = -10, \max = 10)$	-1.11 ± 0.09
FWHM (mas)	$\mathcal{U}(\min = 0, \max = 10)$	1.92 ± 0.05
r_0 (mas)	$\mathcal{N}(\mu = 65, \sigma = 5)$	66.89 ± 0.04
$\dot{r}$ (mas hour^{-1})	$\mathcal{U}(\min = 0, \max = 10)$	0.66 ± 0.05
θ (° East of North)	$\mathcal{N}(\mu = 180, \sigma = 5)$	179.24 ± 0.02

scaling of the photosphere distance (z_0) with luminosity as $z_0 \propto L_\nu^{\sim 0.47}$ (Heinz 2006; Zdziarski et al. 2023), this would correspond to a distance of no more than 1-3 mas downstream from the location of the black hole in J1727, which is within the beam of the VLBA observation projected along the jet axis. Here we have assumed that J1727 has a similar opening angle, inclination angle, and jet speed to Cyg X-1. If the inclination of the jet in J1727 is larger than the normalisation in Zdziarski et al. (2023) ($i = 27.5°$) then this distance will be smaller. Since J1727 contains an early K-type dwarf companion (Mata Sánchez et al. 2024), the jet is not absorbed by a strong stellar wind, and thus this is a very conservative upper limit on the distance from the black hole to the jet photosphere.

We also saw no evidence of a systematic shift in the position of the core as the jet faded. We note that we had to correct for a slight offset due to the different phase calibrators for the VLBA and LBA. Subsequent observations with the VLBA later in the outburst as the extended jet contracted and transient ejecta were launched showed no significant shift in the location of the core (Wood et al. in prep.). This suggests that the distance between the photosphere and the central black hole is not significant compared to the size of the restoring beam.

Any core offset in J1727 leads to an increased brightness ratio, which essentially increases the intrinsic jet speed at a given jet inclination (i.e. the brightness ratio curve constraint shifts right in Figure 5). Although we do not believe there is evidence for a significant core offset, here we report the changes for an offset of 1 mas. In such a case the estimated brightness ratio would increase to 7.1 ± 0.8, and $\beta \cos i = 0.36 \pm 0.03$, which would slightly increase the lower limit on the intrinsic jet speed and decrease the upper limit on the jet inclination (see Section 4.3). We emphasize that such a change has no strong impact on the interpretations of this paper.

4.2. Resolved Jet

The VLBA image of J1727 (Figure 2) is the most resolved image of an X-ray binary hard-state jet. Cyg X-1 and GRS 1915+105 are the only other X-ray binaries with a hard-state jet that has been resolved in an image over multiple synthesised beams (Stirling et al. 2001; Dhawan et al. 2000; Ribó et al. 2004). Assuming a distance to J1727 of 2.7 ± 0.3 kpc (Mata Sánchez et al. 2024), the size of the entire resolved jet structure (including the receding jet) was $\sim 110/\sin i$ AU, and the extent of the approaching jet was $\sim 80/\sin i$ AU, or $5 \times 10^8/\sin i\, r_g$ (assuming a black hole mass of $8\, M_\odot$ Kreidberg et al. 2012). X-ray polarisation observations of J1727 with IXPE suggested that the inclination of the inner accretion flow is between $\sim 30° - 60°$ (Veledina et al. 2023). Therefore the physical extent of the approaching resolved jet of J1727 on 2023 August 30th is between $\sim 95 - 160$ AU, or $\sim (0.6 - 1) \times 10^9\, r_g$.

The two-sided jets of both GRS 1915+105 and Cyg X-1 have been resolved at 8.4 GHz (Dhawan et al. 2000; Ribó et al. 2004; Miller-Jones et al. 2021). The approaching jet of Cyg X-1 has been detected out to an extent of ~ 50 AU (Stirling et al. 2001; Miller-Jones et al. 2021). In 1997, the approaching jet of GRS 1915+105 was detected out to ~ 16 AU (updated with the most recent distance constraint; Dhawan et al. 2000; Reid & Miller-Jones 2023), and in 2003 the jet was measured to be $\lesssim 150$ AU (Ribó et al. 2004, with the upper limit due to interstellar scatter broadening). The approaching jet of MAXI J1836-194 (which has a poorly constrained distance and inclination) was marginally resolved at 8.4 GHz during the decay of its 2011 outburst, with an extent of $\sim 7 - 115$ AU (Russell et al. 2014a,b, 2015). The approaching hard-state jet of MAXI J1820+070 was marginally resolved at 15 GHz, corresponding to a physical extent of ~ 3 AU at 8.4 GHz (scaling the size as $z \propto 1/\nu$; Blandford & Königl 1979; Tetarenko et al. 2021).

The hard-state jet of J1727 was detected out to a further extent than the hard-state jets of Cyg X-1, GRS 1915+105 in its 1997 flare, and MAXI J1820+070. De-
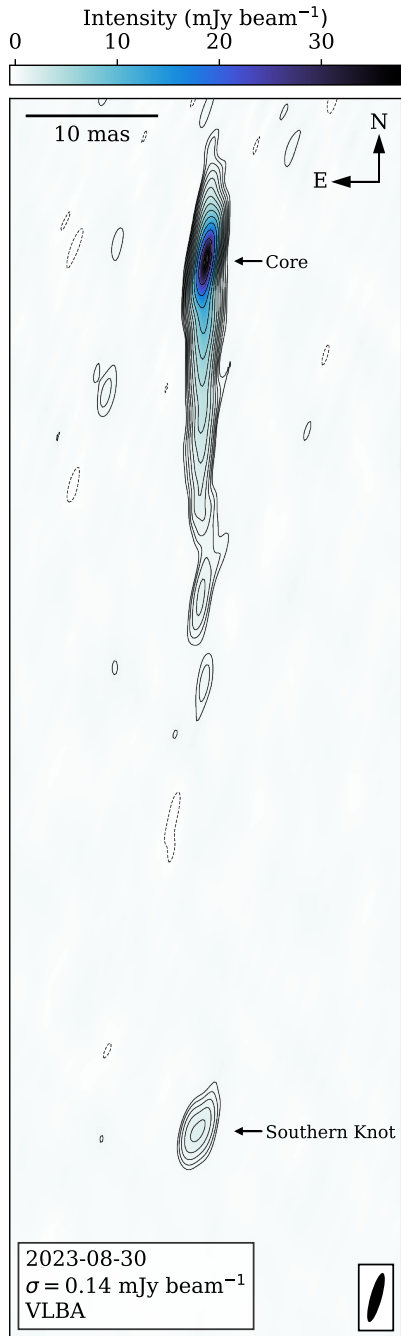
Figure 2. First VLBI image of *Swift* J1727.8-1613 with the VLBA. The contours mark $\pm\sigma \times \sqrt{2}^n$ mJy beam^{-1} where $n = 3, 4, 5, ...$, and σ is the rms noise shown in the lower left of the image. The ellipse in the lower right corner shows the synthesised beam. The image shows a bright core with highly resolved (~ 40 mas) apparently asymmetric bipolar jets extending in the north-south direction, and a discrete jet knot to the south at a separation of 66.7 ± 0.2 mas from the core at a position angle of $179.4 \pm 0.15°$ East of North.

pending on inclination, the resolved hard-state jet of J1727 may also have been larger than the jet of GRS 1915+105 during its 2003 flare, and the decaying hard-state jet of MAXI J1836-194, and therefore J1727 may have had the most extended hard-state jet ever observed in an X-ray binary. The extent of a resolved a hard-state jet is the distance from the core at which the surface brightness of the expanding jet material falls below the noise limit. This depends on both the physical properties of the jet (e.g. opening angle, jet speed, jet content, magnetic field strength, and jet internal structure), as well as the observation parameters, particularly the angular resolution, the overall sensitivity, and the sensitivity to diffuse structure.

Our measured position angle of both the extended jet and the jet knot is consistent with the radio, mm, and X-ray polarisation position angles of J1727, which we compare in Figure 4. These measurements are also consistent with the more poorly constrained optical polarisation orientation (Kravtsov et al. 2023). These measurements suggest that structures in the accretion flow, the jet base, and the downstream jet are aligned to within a few degrees in the plane of the sky.

Between the observations on 2023 August 30th and September 4th and 6th, the extended continuous jet became fainter and less extended, while the core remained relatively constant. We note that the noise level in the observations changes, and thus the distance from the core to which we could detect an identical jet in each observation is different. Our LBA observations did not have sufficient angular resolution and sensitivity to resolve the counter jet, and so we cannot comment on how the jet speed changed as the compact jet faded. We cannot use the lack of a detected counter jet to place a lower limit on the brightness ratio, since the northern jet in the VLBA image can be completely contained within the beam of the subsequent LBA observations. Given the changing resolution of the observations, we also cannot meaningfully compare the peak intensity of the unresolved core across the epochs.

4.3. *Intrinsic Jet Speeds*

Without observing a northern counterpart to the southern jet knot, we cannot uniquely constrain the intrinsic speed and inclination of the source, however we can constrain possible combinations of β and i. The proper motion of the approaching jet knot, μ, is related to the intrinsic speed of the jet knot, β, by,

$$\mu = \frac{\beta \sin i}{1 - \beta \cos i} \frac{c}{d}, \tag{5}$$

where i is the inclination angle of the jet to the line of sight, d is the distance to J1727 (2.7 ± 0.3 kpc; Mata
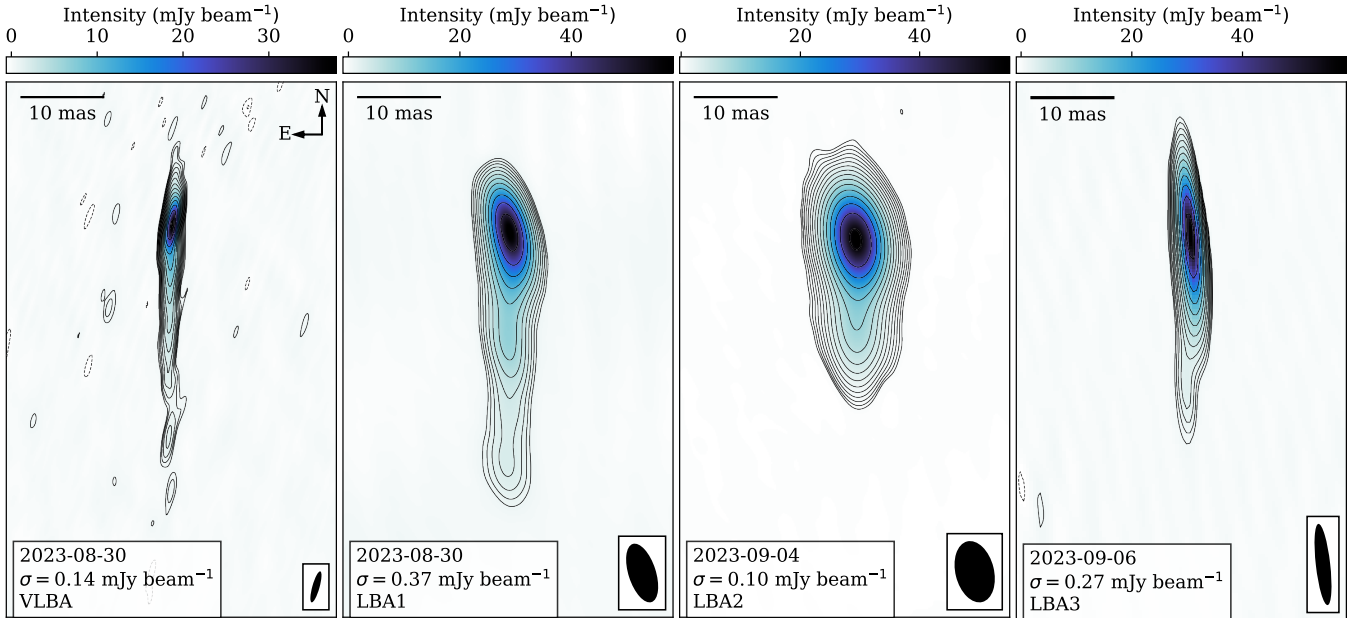
Figure 3. VLBI images of the resolved jet of *Swift* J1727.8-1613 during the hard/hard-intermediate state. The contours mark $\pm\sigma \times \sqrt{2}^n$ mJy beam^{-1} where $n = 3, 4, 5, ...$, and σ is the rms noise shown in the lower left of each image. The ellipse in the lower right corner of each image shows the synthesised beam. The observation parameters can be found in Table 1 and the image parameters can be found in Table 2. The jet is resolved over multiple epochs during the hard state, but appears less extended as the source moves towards the hard-intermediate state.

Sánchez et al. 2024), and c is the speed of light (Mirabel & Rodríguez 1999). We cannot use the non-detection of a receding counterpart to set an upper limit on the flux density ratio to constrain $\beta \cos i$, since we need to measure the flux densities when the jets are at equal separations (i.e. at the same age) since the jets vary in brightness as they move downstream (Miller-Jones et al. 2004).

In Figure 5 we plot the possible values of β and i for both the extended jet and the jet knot, using equations 1 and 5, respectively. These constraints place a lower limit on the intrinsic jet speed of both the continuous and discrete jet knot of $\beta \geq 0.27$ and $\beta \geq 0.2$, respectively. The brightness ratio also gives an upper limit on the jet inclination of $i \leq 74°$. Although they do not have to share the same intrinsic speed, assuming that the discrete jet knot and the continuous extended jet are at the same inclination (i.e. assuming no rapid large-scale precession of the jet axis, as in V404 Cygni; Miller-Jones et al. 2019), then their intrinsic speeds are consistent within 1σ in the interval $i \sim 27 - 37°$. In the inclination range favoured by X-ray polarisation measurements ($i \sim 30° - 60°$; Veledina et al. 2023), the jet knot is moving at the same speed or slower than the continuous jet.

4.4. *Southern Jet Knot*

While the nature of the jet knot is unclear, there are multiple potential scenarios. The most likely explana-

tion is that the jet knot is the result of in-situ particle acceleration in the downstream continuous jet which produced synchrotron emission. Although the approaching extended jet expanded and faded beyond detection at a separation of ~ 30 mas, the jet material will continue to propagate downstream until it loses its energy and momentum to the surrounding medium. An internal shock could be the result of the collision of fast-moving jet material with previously ejected slower-moving jet material. Internal shock models have been used in the past to explain both compact steady jets and discrete transient jets (Jamil et al. 2010; Malzac 2014; Malzac et al. 2018). A short lived internal shock could explain why the jet knot was fading rapidly and was not seen in subsequent observations. This model only requires a change in the jet speed of the continuous jet as it extends outwards during the rise of the outburst. In this scenario, the jet knot does not have to be travelling at the same speed as the continuous jet.

Alternatively, the particle acceleration could be due to a collision between the continuous jet and a dense interstellar medium (ISM). The discrete knot may have then been the 'leading edge' of the extended jet as it advanced outwards through the ISM. Under this scenario, and assuming ballistic motion, the continuous jet would have began extending outwards from the core on MJD 60181.8 ± 0.2, which coincides with the peak of the initial hard-state X-ray rise. If the jet knot was deceler-

Miller-Jones et al. 2012; Russell et al. 2019; Homan et al. 2020; Wood et al. 2021). J1727 did exhibit many of these behaviours later in the outburst during the state transition, however, despite relatively intensive monitoring, no such clear signature of ejection was identified at the beginning of the outburst. An explanation for the jet knot that involves the re-acceleration of material in the out-flowing continuous jet does not require the ejection of a discrete transient jet knot during the hard/hard-intermediate state, and is more consistent with the current understanding of jet evolution during BH LMXB outbursts.

REFERENCES

Astropy Collaboration, Robitaille, T. P., Tollerud, E. J., et al. 2013, A&A, 558, A33, doi: 10.1051/0004-6361/201322068

Astropy Collaboration, Price-Whelan, A. M., Sipőcz, B. M., et al. 2018, AJ, 156, 123, doi: 10.3847/1538-3881/aabc4f

Astropy Collaboration, Price-Whelan, A. M., Lim, P. L., et al. 2022, ApJ, 935, 167, doi: 10.3847/1538-4357/ac7c74

Baglio, M. C., Casella, P., Testa, V., et al. 2023, The Astronomer's Telegram, 16225, 1

Bahramian, A., Tremou, E., Tetarenko, A. J., et al. 2023, ApJL, 948, L7, doi: 10.3847/2041-8213/accde1

Blandford, R. D., & Königl, A. 1979, ApJ, 232, 34, doi: 10.1086/157262

Bright, J., Farah, W., Fender, R., et al. 2023, The Astronomer's Telegram, 16228, 1

Bright, J. S., Fender, R. P., Motta, S. E., et al. 2020, Nature Astronomy, 4, 697, doi: 10.1038/s41550-020-1023-5

Carotenuto, F., Tetarenko, A. J., & Corbel, S. 2022, MNRAS, 511, 4826, doi: 10.1093/mnras/stac329

Castro-Tirado, A. J., Sanchez-Ramirez, R., Caballero-Garcia, M. D., et al. 2023, The Astronomer's Telegram, 16208, 1

Chael, A. A., Johnson, M. D., Bouman, K. L., et al. 2018, ApJ, 857, 23, doi: 10.3847/1538-4357/aab6a8

Charlot, P., Jacobs, C. S., Gordon, D., et al. 2020, A&A, 644, A159, doi: 10.1051/0004-6361/202038368

Chaty, S., Dubus, G., & Raichoor, A. 2011, A&A, 529, A3, doi: 10.1051/0004-6361/201015589

Corbel, S., Fender, R. P., Tzioumis, A. K., et al. 2000, A&A, 359, 251, doi: 10.48550/arXiv.astro-ph/0003460

—. 2002, Science, 298, 196, doi: 10.1126/science.1075857

Corbel, S., Kaaret, P., Fender, R. P., et al. 2005, ApJ, 632, 504, doi: 10.1086/432499

Deller, A. T., Tingay, S. J., Bailes, M., & West, C. 2007, PASP, 119, 318, doi: 10.1086/513572

Deller, A. T., Brisken, W. F., Phillips, C. J., et al. 2011, PASP, 123, 275, doi: 10.1086/658907

Dhawan, V., Mirabel, I. F., & Rodríguez, L. F. 2000, ApJ, 543, 373, doi: 10.1086/317088

Dovciak, M., Ratheesh, A., Tennant, A., & Ma, G. 2023, The Astronomer's Telegram, 16242, 1

Echiburú-Trujillo, C., Tetarenko, A. J., Haggard, D., et al. 2024, ApJ, 962, 116, doi: 10.3847/1538-4357/ad1a10

Espinasse, M., Corbel, S., Kaaret, P., et al. 2020, ApJL, 895, L31, doi: 10.3847/2041-8213/ab88b6

Fender, R. P. 2001, MNRAS, 322, 31, doi: 10.1046/j.1365-8711.2001.04080.x

Fender, R. P., Belloni, T. M., & Gallo, E. 2004, MNRAS, 355, 1105, doi: 10.1111/j.1365-2966.2004.08384.x

Fender, R. P., Homan, J., & Belloni, T. M. 2009, MNRAS, 396, 1370, doi: 10.1111/j.1365-2966.2009.14841.x

Foreman-Mackey, D. 2016, The Journal of Open Source Software, 1, 24, doi: 10.21105/joss.00024

Gandhi, P., Blain, A. W., Russell, D. M., et al. 2011, ApJL, 740, L13, doi: 10.1088/2041-8205/740/1/L13

Greisen, E. W. 2003, in Astrophysics and Space Science Library, Vol. 285, Information Handling in Astronomy - Historical Vistas, ed. A. Heck, 109, doi: 10.1007/0-306-48080-8_7

Harris, C. R., Millman, K. J., van der Walt, S. J., et al. 2020, Nature, 585, 357, doi: 10.1038/s41586-020-2649-2

Heinz, S. 2006, ApJ, 636, 316, doi: 10.1086/497954

Hjellming, R. M., & Rupen, M. P. 1995, Nature, 375, 464, doi: 10.1038/375464a0

Högbom, J. A. 1974, A&AS, 15, 417

Homan, J., Bright, J., Motta, S. E., et al. 2020, ApJL, 891, L29, doi: 10.3847/2041-8213/ab7932

Hunter, J. D. 2007, Computing in Science & Engineering, 9, 90, doi: 10.1109/MCSE.2007.55

Ingram, A., Bollemeijer, N., Veledina, A., et al. 2023, arXiv e-prints, arXiv:2311.05497, doi: 10.48550/arXiv.2311.05497

Jamil, O., Fender, R. P., & Kaiser, C. R. 2010, MNRAS, 401, 394, doi: 10.1111/j.1365-2966.2009.15652.x

Kalamkar, M., Casella, P., Uttley, P., et al. 2016, MNRAS, 460, 3284, doi: 10.1093/mnras/stw1211

Kennea, J. A., & Swift Team. 2023, GRB Coordinates Network, 34540, 1

Kluyver, T., Ragan-Kelley, B., Pérez, F., et al. 2016, in Positioning and Power in Academic Publishing: Players, Agents and Agendas, ed. F. Loizides & B. Schmidt, IOS Press, 87 – 90

Kravtsov, V., Nitindala, A. P., Veledina, A., et al. 2023, The Astronomer's Telegram, 16245, 1

Kreidberg, L., Bailyn, C. D., Farr, W. M., & Kalogera, V. 2012, ApJ, 757, 36, doi: 10.1088/0004-637X/757/1/36

Malzac, J. 2014, MNRAS, 443, 299, doi: 10.1093/mnras/stu1144

Malzac, J., Kalamkar, M., Vincentelli, F., et al. 2018, MNRAS, 480, 2054, doi: 10.1093/mnras/sty2006

Markoff, S., Falcke, H., & Fender, R. 2001, A&A, 372, L25, doi: 10.1051/0004-6361:20010420

Mata Sánchez, D., Muñoz-Darias, T., Armas Padilla, M., Casares, J., & Torres, M. A. P. 2024, A&A, 682, L1, doi: 10.1051/0004-6361/202348754

Matsuoka, M., Kawasaki, K., Ueno, S., et al. 2009, PASJ, 61, 999, doi: 10.1093/pasj/61.5.999

Migliori, G., Corbel, S., Tomsick, J. A., et al. 2017, MNRAS, 472, 141, doi: 10.1093/mnras/stx1864

Miller-Jones, J. C. A., Blundell, K. M., & Duffy, P. 2004, ApJL, 603, L21, doi: 10.1086/382954

Miller-Jones, J. C. A., Jonker, P. G., Ratti, E. M., et al. 2011a, MNRAS, 415, 306, doi: 10.1111/j.1365-2966.2011.18704.x

Miller-Jones, J. C. A., Sivakoff, G. R., Bahramian, A., & Russell, T. D. 2023, The Astronomer's Telegram, 16211, 1

Miller-Jones, J. C. A., Sivakoff, G. R., Altamirano, D., et al. 2011b, in Jets at All Scales, ed. G. E. Romero, R. A. Sunyaev, & T. Belloni, Vol. 275, 224–232, doi: 10.1017/S1743921310016078

Miller-Jones, J. C. A., Sivakoff, G. R., Altamirano, D., et al. 2012, MNRAS, 421, 468, doi: 10.1111/j.1365-2966.2011.20326.x

Miller-Jones, J. C. A., Tetarenko, A. J., Sivakoff, G. R., et al. 2019, Nature, 569, 374, doi: 10.1038/s41586-019-1152-0

Miller-Jones, J. C. A., Bahramian, A., Orosz, J. A., et al. 2021, Science, 371, 1046, doi: 10.1126/science.abb3363

Mirabel, I. F., & Rodríguez, L. F. 1994, Nature, 371, 46, doi: 10.1038/371046a0

—. 1999, ARA&A, 37, 409, doi: 10.1146/annurev.astro.37.1.409

Nakajima, M., Negoro, H., Serino, M., et al. 2023, The Astronomer's Telegram, 16206, 1

Negoro, H., Serino, M., Nakajima, M., et al. 2023a, GRB Coordinates Network, 34544, 1

—. 2023b, The Astronomer's Telegram, 16205, 1

O'Connor, B., Hare, J., Younes, G., et al. 2023a, GRB Coordinates Network, 34549, 1

—. 2023b, The Astronomer's Telegram, 16207, 1

Page, K. L., Dichiara, S., Gropp, J. D., et al. 2023, GRB Coordinates Network, 34537, 1

Péault, M., Malzac, J., Coriat, M., et al. 2019, MNRAS, 482, 2447, doi: 10.1093/mnras/sty2796

Prabu, S., Miller-Jones, J. C. A., Bahramian, A., et al. 2023, MNRAS, 525, 4426, doi: 10.1093/mnras/stad2570

Pradel, N., Charlot, P., & Lestrade, J. F. 2006, A&A, 452, 1099, doi: 10.1051/0004-6361:20053021

Reid, M. J., & Miller-Jones, J. C. A. 2023, ApJ, 959, 85, doi: 10.3847/1538-4357/acfe0c

Reid, M. J., Menten, K. M., Zheng, X. W., et al. 2009, ApJ, 700, 137, doi: 10.1088/0004-637X/700/1/137

Ribó, M., Dhawan, V., & Mirabel, I. F. 2004, in European VLBI Network on New Developments in VLBI Science and Technology, 111–112, doi: 10.48550/arXiv.astro-ph/0412657

Russell, T. D., Soria, R., Miller-Jones, J. C. A., et al. 2014a, MNRAS, 439, 1390, doi: 10.1093/mnras/stt2498

Russell, T. D., Soria, R., Motch, C., et al. 2014b, MNRAS, 439, 1381, doi: 10.1093/mnras/stt2480

Russell, T. D., Miller-Jones, J. C. A., Curran, P. A., et al. 2015, MNRAS, 450, 1745, doi: 10.1093/mnras/stv723

Russell, T. D., Tetarenko, A. J., Miller-Jones, J. C. A., et al. 2019, ApJ, 883, 198, doi: 10.3847/1538-4357/ab3d36

Russell, T. D., Lucchini, M., Tetarenko, A. J., et al. 2020, MNRAS, 498, 5772, doi: 10.1093/mnras/staa2650

Ryle, Martin, S., & Longair, M. S. 1967, MNRAS, 136, 123, doi: 10.1093/mnras/136.2.123

Scheuer, P. A. G., & Readhead, A. C. S. 1979, Nature, 277, 182, doi: 10.1038/277182a0

Skilling, J. 2006, Bayesian Analysis, 1, 833 , doi: 10.1214/06-BA127

Speagle, J. S. 2020, MNRAS, 493, 3132, doi: 10.1093/mnras/staa278

Stirling, A. M., Spencer, R. E., de la Force, C. J., et al. 2001, MNRAS, 327, 1273, doi: 10.1046/j.1365-8711.2001.04821.x

Tetarenko, A. J., Casella, P., Miller-Jones, J. C. A., et al. 2019, MNRAS, 484, 2987, doi: 10.1093/mnras/stz165

—. 2021, MNRAS, 504, 3862, doi: 10.1093/mnras/stab820

Tingay, S. J., Jauncey, D. L., Preston, R. A., et al. 1995, Nature, 374, 141, doi: 10.1038/374141a0

van der Velden, E. 2020, The Journal of Open Source Software, 5, 2004, doi: 10.21105/joss.02004

Veledina, A., Muleri, F., Dovčiak, M., et al. 2023, ApJL, 958, L16, doi: 10.3847/2041-8213/ad0781

Virtanen, P., Gommers, R., Oliphant, T. E., et al. 2020, Nature Methods, 17, 261, doi: 10.1038/s41592-019-0686-2

Vrtilek, S. D., Gurwell, M., McCollough, M., & Rao, R. 2023, The Astronomer's Telegram, 16230, 1

Wells, D. C. 1985, in Data Analysis in Astronomy, ed. V. di Gesu, L. Scarsi, P. Crane, J. H. Friedman, & S. Levialdi, 195

Wenger, M., Ochsenbein, F., Egret, D., et al. 2000, A&AS, 143, 9, doi: 10.1051/aas:2000332

Williams-Baldwin, D., Motta, S., Rhodes, L., et al. 2023, The Astronomer's Telegram, 16231, 1

Wood, C. M., Miller-Jones, J. C. A., Homan, J., et al. 2021, MNRAS, 505, 3393, doi: 10.1093/mnras/stab1479

Wood, C. M., Miller-Jones, J. C. A., Bahramian, A., et al. 2023, MNRAS, 522, 70, doi: 10.1093/mnras/stad939

Woodburn, L., Natusch, T., Weston, S., et al. 2015, PASA, 32, e017, doi: 10.1017/pasa.2015.13

Yang, J., Brocksopp, C., Corbel, S., et al. 2010, MNRAS, 409, L64, doi: 10.1111/j.1745-3933.2010.00948.x

Zdziarski, A. A., Veledina, A., Szanecki, M., et al. 2023, ApJL, 951, L45, doi: 10.3847/2041-8213/ace2c9

APPENDIX

A. HARD-STATE JET PROFILE

To investigate the brightness ratio of the extended jet in Figure 2, we extracted intensity profiles down the northern and southern jets. We first rotated the image of the jet so that it aligns vertically, and then took one dimensional cross sections of the northern and southern jets every 1.05 mas downstream from the core (7 pixels). We fit these cross sections with a one dimensional Gaussian profile to measure the intensity of the approaching and receding jets as a function of separation from the core, which we show in Figure 6. We fitted the Gaussian profiles to the pixel intensities using non-weighted least squares regression with `scipy.optimize.curve_fit`[4], where we report the intensity of the jet as the amplitude of the Gaussian profile. To calculate the uncertainty in the intensity, we added in quadrature the reported 1σ statistical uncertainty from the fit (extracted from the diagonal elements of the covariance matrix), the rms noise in the image, and a 10% calibration error. In Figure 6, we also show the contribution of the unresolved core by taking the one dimensional profile of the restoring beam along the jet axis multiplied by the fit intensity of the core. The contribution from the unresolved core drops below the 5σ limit at a separation of ~ 3 mas. We note that the measurements are correlated along the jet and across the core, since the true intensity profile of the jet is convolved with the Gaussian restoring beam. This explains why the decay of the northern jet is much steeper than the southern jet, since at smaller separations the convolution with the beam across the core causes the intensity to be biased upwards.
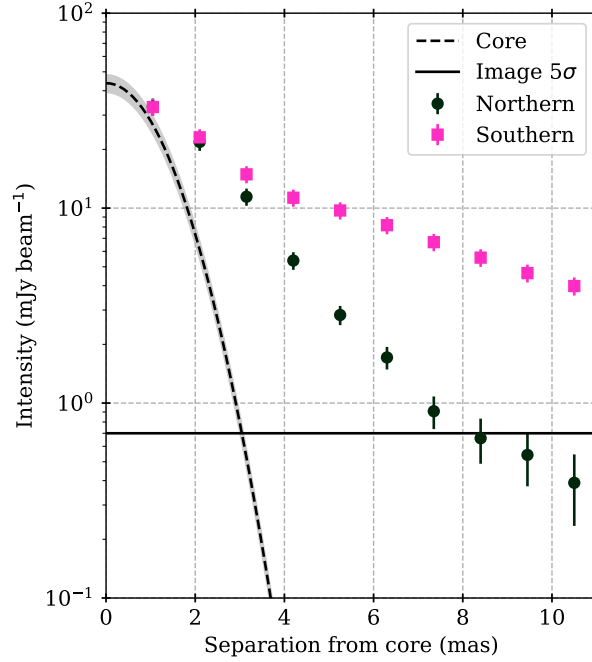

Figure 6. Intensity profile along the northern and southern jet as a function of separation from the core in the VLBA observation of *Swift* J1727.8-1613 shown in Figure 2. The intensity profiles are calculated by fitting 1D Gaussians perpendicular to the jet axis at intervals of ~ 1 mas. The dashed line shows the contribution from the core, calculated by multiplying the intensity of the core by the profile of the restoring beam along the jet axis, with the shaded region showing its uncertainty (derived from the fit).

---

[4] https://docs.scipy.org/doc/scipy/reference/generated/scipy.optimize.curve_fit.html